Design of highly transparent glasses with broadband antireflective subwavelength structures

Young Min Song[1], Hee Ju Choi[2], Jae Su Yu[3], and Yong Tak Lee[1,2,4*]

[1]*Department of Information and Communications, Gwangju Institute of Science and Technology, 1 Oryong-dong, Buk-gu, Gwangju 500-712, Republic of Korea*
[2]*DGraduate Program of Photonics and Applied Physics, Gwangju Institute of Science and Technology, 1 Oryong-dong, Buk-gu, Gwangju 500-712, Republic of Korea*
[3]*Department of Electronic Engineering, Kyung Hee University, 1 Seocheon-dong, Giheung-gu, Yongin-si, Gyeonggi-do 446-701, Republic of Korea*
[4]*Department of Nanobio Materials and Electronics, Gwangju Institute of Science and Technology, 1 Oryong-dong, Buk-gu, Gwangju 500-712, Republic of Korea*
**ytlee@gist.ac.kr*

Abstract: We present a design optimization of highly transparent glasses with broadband antireflective subwavelength structures (SWS) based on the theoretical calculation using a rigorous coupled wave analysis method. It is found that optical transmission characteristics of SWS integrated glasses are governed mainly by the zero-order condition considering multiple internal reflections but not external reflection. By utilizing parabola-shaped SWS on both sides of the glasses with a period of 200 nm and a height of 200 nm, an average transmittance of 99.58% is achieved over a whole range of visible wavelength. Transmission band shrinkage effects of the SWS integrated glass are also observed with increasing the incident angle of light.

©2010 Optical Society of America

OCIS codes: (050.6624) Subwavelength structures; (220.4241) Nanostructure fabrication; (310.6805) Theory and design.

References and links

1. S. Walheim, E. Schaffer, J. Mlynek, and U. Steiner, "Nanophase-separated polymer films as high-performance antireflection coatings," Science **283**(5401), 520–522 (1999).
2. P. Lalanne, and G. M. Morris, "Antireflection behavior of silicon subwavelength periodic structures for visible light," Nanotechnology **8**(2), 53–56 (1997).
3. Y. Kanamori, M. Ishimori, and K. Hane, "High efficient light-emitting diodes with antireflection subwavelength gratings," IEEE Photon. Technol. Lett. **14**(8), 1064–1066 (2002).
4. M. Ishimori, Y. Kanamori, M. Sasaki, and K. Hane, "Subwavelength antireflection gratings for light emitting diodes and photodiodes fabricated by fast atom beam etching," Jpn. J. Appl. Phys. **41**(Part 1, No. 6B), 4346–4349 (2002).
5. Z. Yu, H. Gao, W. Wu, H. Ge, and S. Y. Chou, "Fabrication of large area subwavelength antireflection structures on Si using trilayer resist nanoimprint lithography and liftoff," J. Vac. Sci. Technol. B **21**(6), 2874–2877 (2003).
6. Y.-F. Huang, S. Chattopadhyay, Y.-J. Jen, C.-Y. Peng, T.-A. Liu, Y.-K. Hsu, C.-L. Pan, H.-C. Lo, C. H. Hsu, Y. H. Chang, C.-S. Lee, K.-H. Chen, and L.-C. Chen, "Improved broadband and quasi-omnidirectional anti-reflection properties with biomimetic silicon nanostructures," Nat. Nanotechnol. **2**(12), 770–774 (2007).
7. Y. Li, J. Zhang, S. Zhu, H. Dong, Z. Wang, Z. Sun, J. Guo, and B. Yang, "Bioinspired silicon hollow-tip arrays for high performance broadband anti-reflective and water-repellent coatings," J. Mater. Chem. **19**(13), 1806–1810 (2009).
8. Y. M. Song, E. S. Choi, J. S. Yu, and Y. T. Lee, "Light-extraction enhancement of red AlGaInP light-emitting diodes with antireflective subwavelength structures," Opt. Express **17**(23), 20991–20997 (2009).
9. P. Yu, C.-H. Chang, C.-H. Chiu, C.-S. Yang, J.-C. Yu, H.-C. Kuo, S.-H. Hsu, and Y.-C. Chang, "Efficiency enhancement of GaAs photovoltaics employing antireflective indium tin oxide nanocolums," Adv. Mater. **21**(16), 1618–1621 (2009).
10. S. Wang, X. Z. Yu, and H. T. Fan, "Simple lithographic approach for subwavelength structure antireflection," Appl. Phys. Lett. **91**(6), 061105 (2007).
11. Y. M. Song, S. J. Jang, J. S. Yu, and Y. T. Lee, "Bioinspired parabola subwavelength structures for improved broadband antireflection," Small **6**(9), 984–987 (2010).
12. A. Gombert, W. Glaubitt, K. Rose, J. Dreibholz, B. Blasi, A. Heinzel, D. Sporn, W. Doll, and V. Wittwer, "Subwavelength-structured antireflective surfaces on glass," Thin Solid Films **351**(1-2), 73–78 (1999).

#127956 - $15.00 USD Received 4 May 2010; revised 28 May 2010; accepted 28 May 2010; published 2 Jun 2010
(C) 2010 OSA

13. Y. Kanamori, H. Kikuta, and K. Hane, "Broadband antireflection gratings for glass substrates fabricated by fast atom beam etching," Jpn. J. Appl. Phys. **39**(Part 2, No. 7B), L735–L737 (2000).
14. K. Kintaka, J. Nishii, A. Mizutani, H. Kikuta, and H. Nakano, "Antireflection microstructures fabricated upon fluorine-doped SiO_2 films," Opt. Lett. **26**(21), 1642–1644 (2001).
15. W.-L. Min, B. Jiang, and P. Jiang, "Bioinspired self-cleaning antireflection coatings," Adv. Mater. **20**(20), 3914–3918 (2008).
16. Y. H. Kang, S. S. Oh, Y.-S. Kim, and C.-G. Choi, "Fabrication of antireflection nanostructures by hybrid nano-patterning lithography," Microelectron. Eng. **87**(2), 125–128 (2010).
17. M. Ibn-Elhaj, and M. Schadt, "Optical polymer thin films with isotropic and anisotropic nano-corrugated surface topologies," Nature **410**(6830), 796–799 (2001).
18. Z. Wu, J. Walish, A. Nolte, L. Zhai, R. E. Cohen, and M. F. Rubner, "Deformable antireflection coatings from polymer and nanoparticle multilayers," Adv. Mater. **18**(20), 2699–2702 (2006).
19. W. H. Southwell, "Gradient-index antireflection coatings," Opt. Lett. **8**(11), 584–586 (1983).
20. E. Hecht, *Optic 4th ed.*(Addison Wesley, 2002), Chap. 10.
21. H. Y. Koo, D. K. Yi, S. J. Yoo, and D.-Y. Kim, "A snowman-like array of colloidal dimmers for antireflecting surfaces," Adv. Mater. **16**(3), 274–277 (2004).
22. M. A. Ray, N. Shewmon, S. Bhawalkar, L. Jia, Y. Yang, and E. S. Daniels, "Submicrometer surface patterning using interfacial colloidal particle self-assembly," Langmuir **25**(13), 7265–7270 (2009).

1. Introduction

In the last few decades, steady efforts have been made to achieve broadband antireflection characteristics for various optical components. Even though antireflection coatings (ARCs) using multilayer thin-film stacks are widely used, there still exist many problems associated with material selection, band limitation, and thermal mismatch between the film and the substrate [1,2]. Recently, antireflective subwavelength structures (SWS) directly patterned on a substrate as an alternative to multilayer ARCs has attracted growing interest due to their ultra-broadband and omni-directional antireflection properties [3–15]. Moreover, water-repellent surfaces of SWS enable applications in humidity sensitive environments. SWS surfaces were fabricated on a variety of semiconductor materials, such as silicon, GaAs, GaSb, GaP, and GaN, to increase the optical efficiency in optoelectronic device applications including solar cells, photodetectors, and light-emitting-diodes [3–11]. Additionally, transparent glasses and polymer films as an optical substrate are essential for displays, projection optical devices, and eye glasses [12–18]. Although the refractive index of glasses is not as much as that of semiconductor materials, its discontinuity between air and glass serves only ~92% of total transmittance, which degrades the performance of optical devices.

To fabricate SWS on glass substrate, many methodological approaches, such as e-beam/ interference lithography, nanoimprint lithography, colloidal self assembly, and metal nanoparticles, have been developed [12–16]. However, only few theoretical approaches for SWS integrated glasses were reported. In solar cells and other photosensitive devices, the incident light experiences external reflection at air-substrate interface. On the other hand, in glass, the light experiences multiple 'internal' reflections to pass through top and bottom interfaces. This difference is very crucial to determine the period, height and shape of SWS because the light diffraction from the grating structure depends on the refractive index of the incident medium. In this work, we designed highly transparent glasses with single and double-side SWS by considering multiple internal reflections. The period, height and shape of SWS were optimized to achieve high transmittance over a wide wavelength range using a rigorous coupled-wave analysis (RCWA) method. For some SWS fabricated on glass substrates, the experimentally measured transmission data were compared with the results from the theoretical calculation.

2. Simulations and SWS geometries

First, we have calculated the reflection efficiency for the four kinds of SWS, i.e., nanorod, truncated cone, perfect cone, and paraboloid, to optimize the SWS geometrically. To calculate the reflectance of SWS on glass substrate, a three-dimensional RCWA simulation method was employed. In this calculation, the grating period of SWS was fixed to 100 nm, which is small enough to obtain only the zero-order diffraction in grating structures, and the height was varied from 0 to 400 nm. For all structures, a six-fold hexagonal symmetry was used and the

#127956 - $15.00 USD Received 4 May 2010; revised 28 May 2010; accepted 28 May 2010; published 2 Jun 2010
(C) 2010 OSA

dispersion of glass (BoroFloat 33, Schomit) was taken into account. The diameter of nanorod structure was set to 50% of its period. In cones and parabolic structures, it was assumed that each structure is closely packed. The apex diameter was set to 50% of the base diameter in the truncated cone. The SWS with cubic or quintic index profile have better antireflection performances than other structures [19], but these are difficult to realize and so are not treated here.

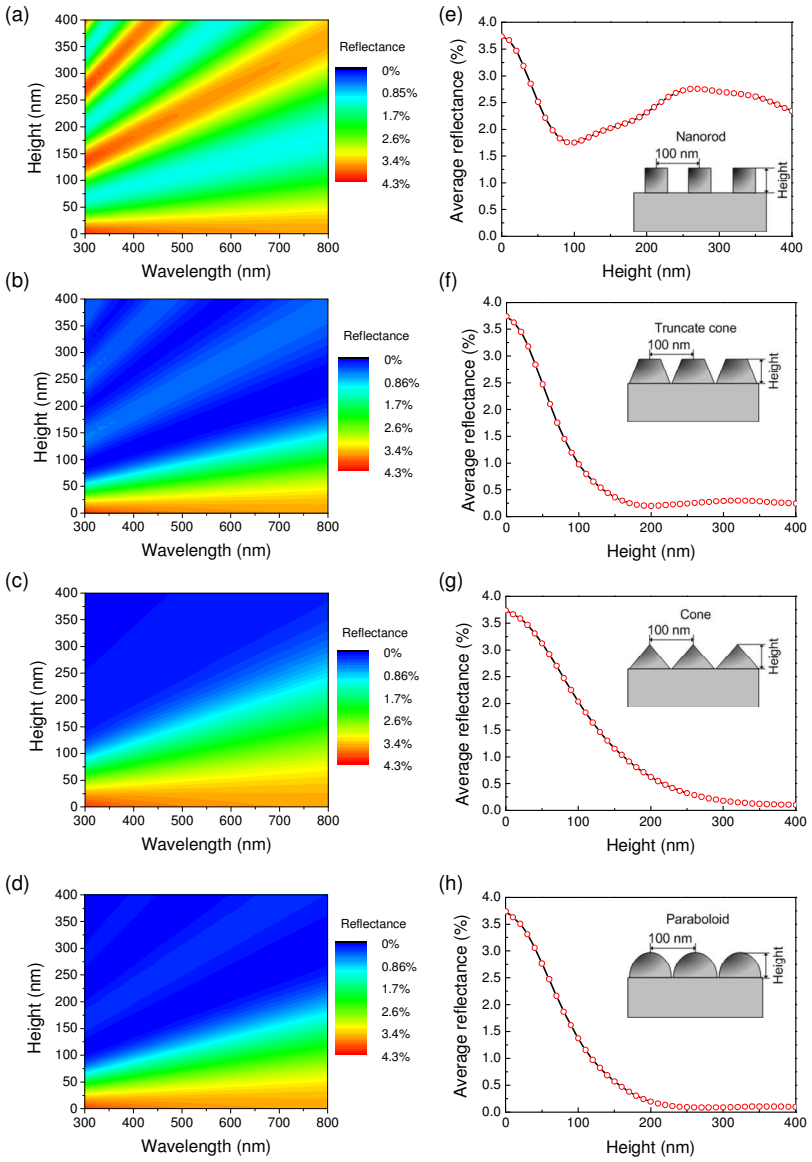

Fig. 1. Contour plot of the calculated reflectance of glass SWS in the shapes of (a) nanorod, (b) truncated cone, (c) perfect cone and (d) paraboloid as a function of height and wavelength at normal incidence for a period of 100 nm. The (e)-(h) corresponds to the average reflectance versus SWS height. The insets of (e)-(h) describe each schematic cross-sectional image.

#127956 - $15.00 USD Received 4 May 2010; revised 28 May 2010; accepted 28 May 2010; published 2 Jun 2010
(C) 2010 OSA

3. Results and discussion

3.1. Design and fabrication of single-side SWS integrated glasses

Figure 1 shows the contour plot of the calculated reflectance of glass SWS in the shapes of (a) nanorod, (b) truncated cone, (c) perfect cone, and (d) paraboloid at normal incidence for a period of 100 nm. Figures 1 (e)-1(h) corresponds to the average reflectance in the wavelength range of 300-800 nm as a function of the SWS height. Each schematic cross-sectional image is also described in the insets of Figs. 1(e)-1(h). The flat surface (height = 0) of glass exhibits the average reflectance of 3.74% as expected. For nanorod SWS, the reflectance is not much smaller than that of the flat surface because the nanorod acts as an effective medium that approximates a single layer thin film. In fact, the optical property of the nanorod with a subwavelength period is quite similar with that of a single layer antireflection coating. At each wavelength, there are fluctuations in reflectance as the height increases due to the interference of light reflected at the top and bottom of the layer. The nanorod shows a low reflectance only in specific wavelength ranges as can be seen in Fig. 1(a). Thus, the nanorod structure is not adequate for broadband antireflection applications. In Figs. 1(b) and 1(d), the SWS with conical shape have lower reflectance than that of the flat surface and nanorod structure. As the height is increased, the reflectance tends to decrease. This can be explained by the fact that the effective refractive index is gradually changed. For example, the SWS with perfect cone provide an average reflectance of 0.10% at the height of 400 nm. The perfect cone is more favorable to obtain low average reflectance than the truncated cone. However, below ~200 nm height, the truncated cone shows better antireflection characteristics. This implies that the rapid change of the effective refractive index rather obstructs the reduction of reflection. Because the effective refractive index in three-dimensional structures with subwavelength periods is determined by the volume fraction, the paraboloid has a nearly linear refractive index profile, which is more efficient to reduce the surface reflection than the cone-shaped structure. As shown in Fig. 1, the SWS with parabolic shape show lowest average reflectance among these structures. This parabola-shaped structure with high packing density can be realized by lens-like shape transfer process [11].

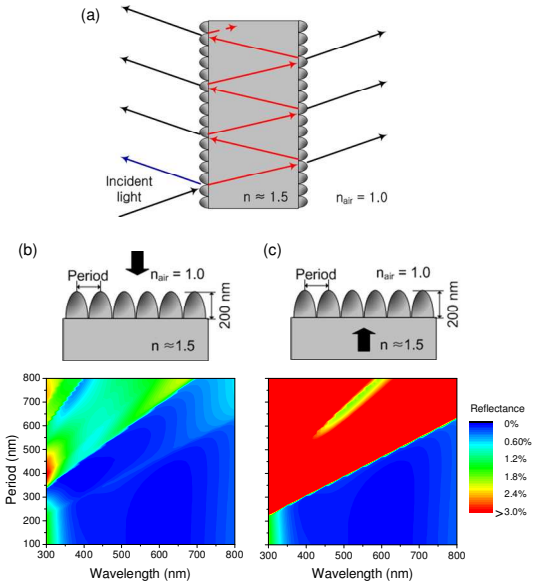

Fig. 2. (a) Schematic diagram of light propagation for the dual-side SWS integrated glass, and contour map of the reflectance for (b) the external reflection from the air to the glass and (c) the internal reflection from the glass to the air as a function of period and wavelength for the height of 200 nm.

#127956 - $15.00 USD Received 4 May 2010; revised 28 May 2010; accepted 28 May 2010; published 2 Jun 2010
(C) 2010 OSA

When the light encounters the front surface of the glass, an external reflection (blue arrow) occurs only once from the SWS. Subsequently, multiple internal reflections (red arrows) occur inside the glass, which is similar with a Fabry-Perot etalon. The schematic diagram of light propagation for the dual-side SWS integrated glass is depicted in Fig. 2(a). In grating structures, the grating period should be at least smaller than the wavelength of incident light in order to act as a nonstructured medium. It is important to note that the cutoff limit period is closely related to the refractive index of incident medium because the angles of the reflected diffraction waves $\theta_{r,m}$ in the m-*th* diffraction are given by the well-known grating equation [20]:

$$\sin\theta_{r,m} = \frac{m\lambda}{\Lambda n} + \sin\theta_i, \tag{1}$$

where n is the refractive index of incident medium, θ_i is the incident angle, and λ is the incident wavelength. In internal reflection, the grating period should be much shorter compared to the conventional external reflection due to the higher refractive index of glass than that of air. Figures 2(b) and 2(c) show the contour plots of the reflectance of SWS with a 200 nm height as a function of wavelength and grating period for external and internal reflections, respectively. In the case of the external reflection, the SWS with the period of 300 nm, which can be easily implemented by the conventional laser interference lithography, are enough to cover the whole visible wavelength range. However, at least ~200 nm period is needed in the internal reflection to eliminate the higher-order diffractions in the wavelength range of 300-800 nm. The gaps of the cutoff period between the external and internal reflections are 140 nm and 220 nm at wavelengths of 400 nm and 700 nm, respectively. If the refractive index of the incident medium is increased, these gaps will be significantly widened.

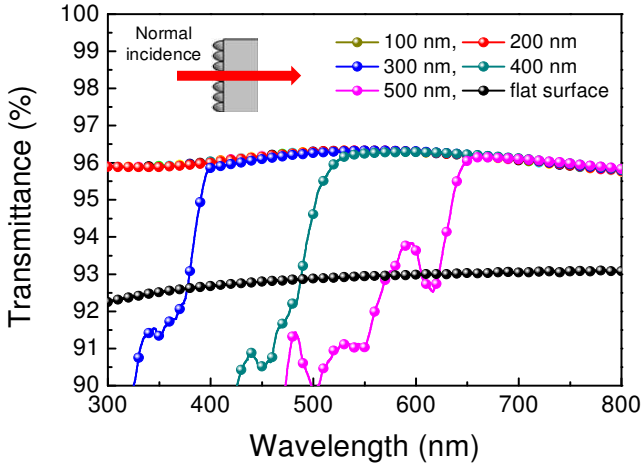

Fig. 3. Calculated transmittance spectra of single-side SWS integrated glasses with different grating periods at normal incidence. Calculated transmittance of dual-side polished glass is shown as a reference.

To investigate the effect of period in SWS integrated glasses, the transmittance calculations were carried out for SWS integrated glasses with different grating periods. For glasses with SWS on the top surface, the height of SWS was fixed at 200 nm on 100 μm thick substrate in this calculation. The calculated values at each wavelength were averaged to remove rapid fluctuations caused by the interference of light reflected at the top and bottom surface. Figure 3 shows the calculated transmittance spectra of single-side SWS integrated

#127956 - $15.00 USD Received 4 May 2010; revised 28 May 2010; accepted 28 May 2010; published 2 Jun 2010
(C) 2010 OSA

glasses with different grating periods at normal incidence. The grating period was varied from 100 nm to 500 nm by a step of 100 nm. For comparison, the calculated transmittance of a dual-side polished glass is also shown as a reference. The glasses with single-side SWS yield transmittance of ~96% due to the graded refractive index profiles, while it is only ~93% for the flat surface. For the periods of 100 nm and 200 nm, the transmittance curves of the SWS integrated glasses are almost the same, with sustaining high values over a wide wavelength range of 300-800 nm. Above 300 nm period, however, it exhibited a rapid drop of the transmittance at specific wavelengths, which is attributed to the higher order diffraction. Interestingly, the drop points of the SWS integrated glasses with periods of 300 nm, 400 nm, and 500 nm are ~390 nm, ~510 nm, and ~640 nm, respectively. They are consistent with cutoff points at each wavelength as shown in Fig. 2(c). This indicates that the transmittance of the SWS integrated glasses is not dependant on the external reflection but on the internal reflection.

In order to confirm experimentally the above results, we fabricated the single-side SWS integrated glasses. For the fabrication of SWS on glass substrate, a diluted photoresist (PR) was spin-coated on the glass substrate (BoroFloat 33, Schomit). After prebaking on a hot plate at 90 °C for 90 s, the PR was then exposed twice by the interference of two beams using an Ar laser operating at wavelength of 363.8 nm to form two-dimensional periodic PR patterns. The period of the grating can be changed by adjusting an angle of Lloyd's mirror. For hexagonal patterns, the sample was rotated by 60 degree between each exposure. After the development, the PR patterned glass was etched by using reactive ion etcher under the process pressure of 50 mTorr and the rf power of 50 W. CF_4 gas with flow rate of 50 sccm was used to etch the glass substrate. After removal of PR and cleaning of the sample, the etched profile of the fabricated SWS on glass was observed by using scanning electron microscope (SEM). The optical transmittance at normal incidence was measured by using UV-VIS-NIR spectrophotometer.

Figure 4 shows the measured transmittance of the fabricated SWS on glass substrates with periods of 300 nm and 400 nm as a function of wavelength at normal incidence. The inset shows the 45 degree tilted view of SEM images for the fabricated SWS. Measured transmittance of dual-side polished glass is shown as a reference, indicating a similar curve with the theoretical prediction except for the wavelength ranges below ~400 nm. This difference is caused by the strong light absorption of glasses at wavelengths below ~400 nm. The gaps of ~0.6% between the calculated and experimental transmittances of glass with flat surface are probably attributed to the mismatch of refractive indices of the glass used in this calculation. Because the shape of the fabricated SWS somewhat deviates from ideal geometry, the measured transmittance is lower than the theoretically calculated results. Despite of this discrepancy, the tendency (i.e., drop points related to the grating period) is in reasonable agreement with our expectation. This phenomenon can be found in other literatures [21,22], but it was not clearly explained. As shown in Fig. 3, the high transmittance characteristics can be extended even to shorter wavelengths by implementing sub-200 nm period patterning. Unfortunately, it is difficult to find optimum condition to obtain sub-200 nm period grating patterns by using laser interference lithography. The SWS with sub-200 nm period can be fabricated by nano patterning techniques such E-beam lithography, colloidal formation, and metal nanoparticles.

#127956 - $15.00 USD Received 4 May 2010; revised 28 May 2010; accepted 28 May 2010; published 2 Jun 2010
(C) 2010 OSA

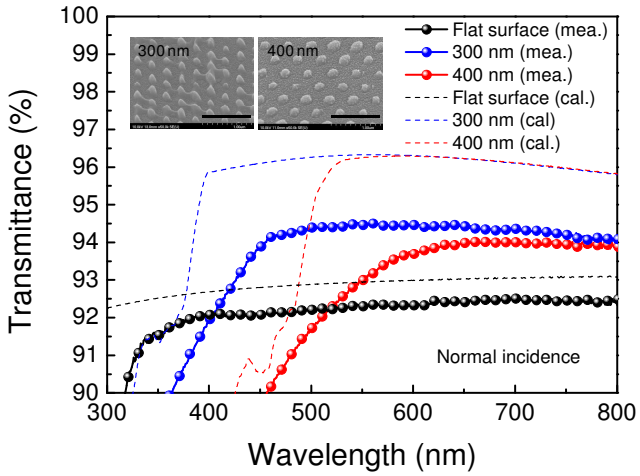

Fig. 4. Measured transmittance of the fabricated SWS on glass substrates with different periods as a function of wavelength at normal incidence. Inset shows the SEM images of the fabricated SWS on glass substrate with period of 300 nm and 400 nm. Scale bar of SEM images corresponds to 1 μm. Measured transmittance of dual-side polished glass is shown as a reference. The dashed lines show the calculated curves.

3.2. Design of dual-side SWS integrated glasses

Nearly 100% transmission of light can be achieved by applying the SWS on both sides of the glass substrate. Figure 5(a) shows the calculated transmittance of dual-side SWS integrated glasses with different grating periods at normal incidence. The grating height was fixed to 200 nm in this calculation. Dual-side SWS integrated glasses with below 200 nm period show an average transmittance of 99.58% at wavelengths of 300-800 nm. Maximum transmittance is 99.99% at 530 nm wavelength as can be expected in Fig. 1(d). Note that, for the periods above 300 nm, there are rapid drops at the same positions as those of the single-side SWS integrated glasses. These results provide a possibility for wavelength selection simply by adjusting the period of SWS. To obtain ultra-broadband antireflection property in SWS, taller features as well as fine structures are needed. Figure 5(b) shows the effect of grating height on the transmittance spectra of dual-side SWS integrated glasses at normal incidence. Despite different grating periods, the SWS with the same heights produce the same transmittance curves above the wavelength satisfying the zero-order condition as shown in Fig. 5(b). At the height of 200 nm, the transmittance of the SWS maintained over 99.5% at short wavelength regions, but it decays gradually as the wavelength increases and then goes down to 99% above 750 nm wavelength. When the height is increased from 200 nm to 300 nm, the transmittance of > 99% is maintained until the wavelength reaches 1100 nm. The dual-side SWS integrated glass with a period of 200 nm and a height of 400 nm (i.e., aspect ratio of 2) leads to the average transmittance of 99.84% over a wide wavelength range of 300-1200 nm. From this point of view, nanoscale hollow tip arrays with a tip height up to 1 um, which are successfully demonstrated on silicon substrate by several research groups [6,7], are desirable for ultra-broadband antireflection. In general, the dry etch process for achieving high aspect ratios is very difficult, especially in glasses and other transparent films. Hence, for a specific application, the grating period and height should be carefully chosen according to these plots.

#127956 - $15.00 USD Received 4 May 2010; revised 28 May 2010; accepted 28 May 2010; published 2 Jun 2010
(C) 2010 OSA

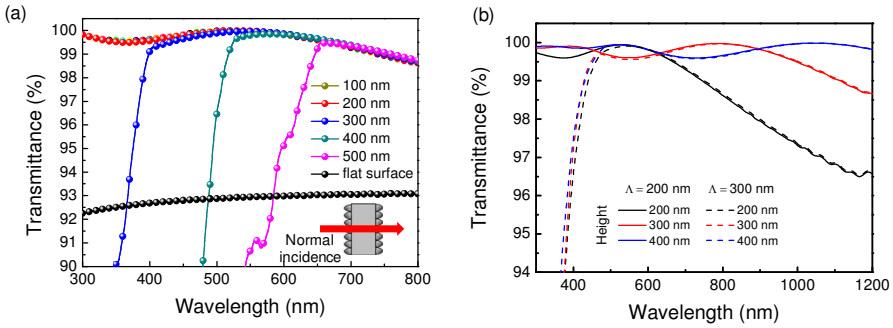

Fig. 5. Calculated transmittance spectra of dual-side SWS integrated glasses at normal incidence (a) with different grating periods and (b) with different grating heights. Calculated transmittance of dual-side polished glass is shown in (a) as a reference.

Incident angle of light is also closely related to the zero-order condition as seen from Eq. (1). When the incident angle is increased, the grating period should be shortened to satisfy the zero-order condition. Figure 6(a) illustrates the angle dependent transmittance spectra of bare glass and dual-side SWS integrated glass with a period of 300 nm and a height of 200 nm. The incident angle is changed from 0 o to 50° by a step of 10°. In calculation of angle dependent transmittance, plane waves with a fixed polarization angle of 45° were used as the incident light instead of a randomly polarized light. As the incident angle increases, the transmittance of both bare glass and dual-side SWS integrated glass are decreased due to the enhanced Fresnel reflection. While the angle dependent transmittance for bare glass does not rely on the wavelength, the transmittance spectra of SWS integrated glass reveals unusual curves below specific wavelengths. Owing to the decreased cutoff period, the drop points are shifted toward the longer wavelength. This fact is inevitable and crucial to determine the grating period in the design of the SWS on glasses considering the spectral band of interest. As shown in Fig. 6(b), the wavelength shift of 30-40 nm occurs as the incident angle increases by a step of 10°. As a result, the period of 300 nm is not adequate for angle-independent transparent glasses. On the contrary, this structure can be used for the purpose of the angle-dependent wavelength selection. The slope (i.e., wavelength over incident angle) of the SWS with the period of 200 nm exhibits a similar tendency. For the grating period of 200 nm, the whole visible range can be covered only at incident angles below 40°. Therefore, the SWS with periods of < 200 nm are required for angle-independent highly transparent glasses.

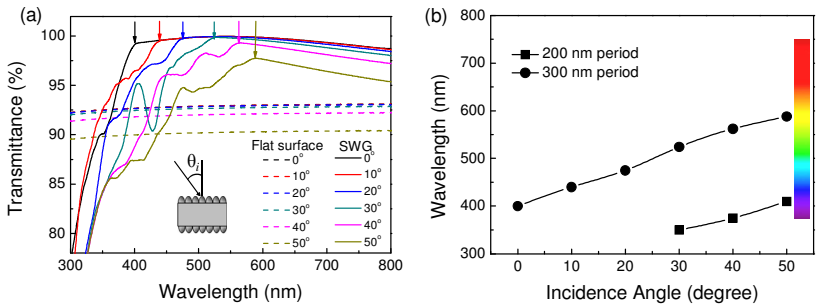

Fig. 6. (a) Angle dependent transmittance spectra of bare glass with flat surface (dashed line) and dual-side SWS integrated glass with a period of 300 nm and a height of 200 nm (solid line) for θ_i = 0, 10, 20, 30, 40, and 50°. Arrows indicate the drop points of each transmittance curve. (b) Drop points at each incidence angle for the periods of 200 nm (rectangle) and 300 nm (circle).

#127956 - $15.00 USD Received 4 May 2010; revised 28 May 2010; accepted 28 May 2010; published 2 Jun 2010
(C) 2010 OSA

4. Conclusion

In conclusion, we designed the antireflective nanostructures on glass substrates by optimizing the shape and geometry of SWS for near 100% light transmission in a wide wavelength range. From the investigation of various SWS geometries using the RCWA simulation, the paraboloid is proved to be desirable for high transparent glasses. For the fabrication of SWS on glass substrate, the experimental results and theoretical calculations give a reasonable consistency. The parabola-shaped double-side SWS with a period of 200 nm and a height of 200 nm were optimized to guarantee over 99.5% transmittance in visible wavelength ranges. Also, it was found that the period of SWS should be smaller than at least 200 nm to satisfy the zero-order condition in glasses considering internal reflections. We believe that these results may provide fruitful insights to design and fabricate the highly transparent materials with SWS and other related optical devices.

Acknowledgement

This work was partly supported by the GIST Systems Biology Infrastructure Establishment Grant, by the World Class University (WCU) program at GIST through a grant provided by MEST of Korea (R31-20008-000-10026-0), and by the Core Technology Development Program for Next generation Solar Cells of Research Institute for Solar and Sustainable Energies (RISE), GIST. The authors would like to acknowledge Prof. Han Sup Lee and Mr. Kiwoon Choi in Inha University for their fruitful comments and suggestions.

#127956 - $15.00 USD Received 4 May 2010; revised 28 May 2010; accepted 28 May 2010; published 2 Jun 2010
(C) 2010 OSA